THE JOURNAL OF PHYSICAL CHEMISTRY A

Article

pubs.acs.org/JPCA

Configuration-Space Sampling in Potential Energy Surface Fitting: A Space-Reduced Bond-Order Grid Approach

Sergio Rampino*

Istituto di Scienze e Tecnologie Molecolari, Consiglio Nazionale delle Ricerche c/o Dipartimento di Chimica, Biologia e Biotecnologie, Università degli Studi di Perugia, Via Elce di Sotto 8, 06123 Perugia, Italia

ABSTRACT: Potential energy surfaces (PESs) for use in dynamics calculations of few-atom reactive systems are commonly modeled as functional forms fitting or interpolating a set of ab initio energies computed at many nuclear configurations. An automated procedure is here proposed for optimal configuration-space sampling in generating this set of energies as part of the grid-empowered molecular simulator GEMS (Laganà et al., *J. Grid Comput.* **2010**, *8*, 571−586). The scheme is based on a space-reduced formulation of the so-called bond-order variables allowing for a balanced representation of the attractive and repulsive regions of a diatom configuration space. Uniform grids based on space-reduced bond-order variables are proven to outperform those defined on the more conventional bond-length variables in converging the fitted/interpolated PES to the computed ab initio one with increasing number of grid points. Benchmarks are performed on the one- and three-dimensional prototype systems H_2 and H_3 using both a local-interpolation (modified Shepard) and a global-fitting (Aguado−Paniagua) scheme.

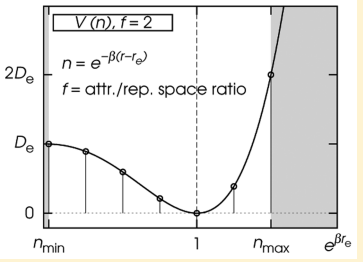

1. INTRODUCTION

The quantum treatment of chemical reaction dynamics in the Born−Oppenheimer regime requires solving the Schrödinger equation for the motion of nuclei on one or a manifold of potential energy surfaces (PESs) associated with the electronic states of a molecular system. The solution of the nuclei Schrödinger equation, which can be cast either in a time-dependent (TD)[1−4] or a time-independent (TI)[5−8] form, is then matched to proper asymptotic conditions to get the elements of the so-called scattering (*S*) matrix,[9] corresponding to the quantum mechanical reaction probability amplitude, out of which observable properties can be extracted to be compared with the outcome of crossed-molecular-beam experiments.[10] Since Schatz and Kuppermann's first calculation on H + H_2 in 1976,[11,12] much progress has been made in the development of rigorous TD and TI methods, and many studies, though mainly limited for computational reasons to three- or four-atom systems, have been published (see refs 13 and 14 for a review of the reactions studied from the early days up to recent times). Recently developed approximate schemes such as the multi-configuration time-dependent Hartree (MCTDH)[15] are likely to extend the range of applicability of the quantum treatment of chemical reactions to systems with many more degrees of freedom.

Ideally, accurate values of the electronic energies should be available at all geometries needed by the dynamics calculations. Examples have been reported of so-called "direct dynamics", whereby the electronic energies are calculated on-the-fly at the geometries needed by the dynamics.[16−18] However, the most usual and efficient approach to dynamics calculations is to formulate the PES using a suitable analytic functional representation. This can either be a semiempirical expression (such as the popular London−Eyring−Polanyi−Sato, LEPS[19−22]) or, more commonly, fit or interpolate a set of energies computed at a number of nuclear configurations by high-level ab initio methods. The topic of analytical representations of PESs, especially with regard to the most suitable functional forms, has been reviewed over the years by Sathyamurthy,[23] Truhlar,[24] Schatz,[25,26] and several others.[27−29] The reader is referred to these works for further details.

Less attention has been paid, instead, to the issue of properly sampling the configuration space when generating the ab initio energies to be fitted or interpolated—in other words, at which geometries the ab initio calculations should be performed. Choosing an as small as possible set of points optimally sampling configuration space is of crucial importance in PES crafting as ab initio calculations are usually computationally highly demanding. Not to mention that some of the points could not converge to the desired state, and the analysis of a wisely reduced set of points could avoid unwanted difficulties[30,31] (after all, this is a good reason for not adopting direct methods). Information on this subject in the cited reviews does not go beyond hints and, as a matter of fact, no general ways of selecting suitable sets of nuclear configurations (besides iterative sampling methods based on classical trajectories[32,33] or successive-degree fitting[34]) have, to the best of the author's knowledge, been published.

We recently came across the issue of choosing the minimum most informative set of ab initio values during the assembly of the grid-empowered molecular simulator GEMS[35−38] for the a priori modeling of elementary reactive processes[39−42] in which

Special Issue: Piergiorgio Casavecchia and Antonio Lagana Festschrift

Received: October 13, 2015
Revised: December 14, 2015
Published: December 16, 2015

DOI: 10.1021/acs.jpca.5b10018
J. Phys. Chem. A 2016, 120, 4683−4692

all the arrangement channels need to be optimally described. GEMS is articulated in four blocks (INTERACTION, FITTING, DYNAMICS, and OBSERVABLES) featuring a high degree of interoperability thanks to the definition of the common data formats Q5Cost/D5Cost.[43,44] The four blocks are part of a workflow designed to enable the coordinated execution of in-house developed and commercial codes on the distributed platform of the European Grid Infrastructure[45] by properly selecting compute resources among the high-performance computing (HPC) and high-throughput computing (HTC) available ones. GEMS has been successfully used to study the dynamics and compute the reactive probabilities/cross sections and rate coefficients of atom−diatom systems such as H + H_2,[44] Li + FH,[42] N + N_2,[46,47] and O + O_2,[48,49] where PESs were already available. However, while electronic-structure and fitting programs are already incorporated into GEMS, an automated procedure for a full generation of the PES including an optimal choice of geometries at which ab initio calculations should be performed is still missing.

In the present paper the issue of optimal configuration-space sampling for PES fitting/interpolation of few-atom reactive systems is addressed. A general and flexible scheme is devised based on a space-reduced (SR) formulation of the so-called bond-order (BO) variables (see Section 2.1), allowing for a balanced representation of the attractive and repulsive regions of a diatom configuration space. Uniform grids in space-reduced bond-order (SRBO) variables are then proven to outperform those defined on the more conventional interatomic distances (or bond-length, BL, variables) in converging the interpolated PES to the computed ab initio one with increasing number of grid points. The procedure is tested and comparatively assessed on the one-dimensional problem of the H_2 bond-dissociation curve and on the three-dimensional one of a reactive PES for the H + H_2→ H_2 + H atom-exchange reaction using both local-interpolation (modified Shepard[50]) and global-fitting (Aguado−Paniagua[51,52]) schemes (see Section 2.2). It should be stressed here that the focus of the paper is that of a critical assessment of the proposed configuration-space sampling scheme rather than the generation of new functional representations for the PESs of the above-mentioned systems. A full application of the procedure to a new case study is to be found in ref 53, where the scheme herein devised is used to compute for the first time the ground-state PES of the C_2H^+ system of interest for interstellar chemistry.

The paper is organized as follows. In Section 2 the methodology is outlined, and computational details are given. Results are presented in Section 3. Conclusions and plans for future work are drawn in Section 4.

2. METHODS AND COMPUTATIONAL DETAILS

As already mentioned in the Introduction, usually the first step in PES generation is the choice of a set of nuclear configurations at which ab initio energies shall be computed to be then fitted to/interpolated by suitable functional forms. For the one-dimensional case of a diatom, a straightforward and rather conventional way is to adopt as coordinate the internuclear distance (or bond-length, BL, variable) r, fix two boundary values r_{min} and r_{max}, and compute the ab initio energies at the points of a uniform grid on the segment of r between r_{min} and r_{max}.

For higher-dimensionality problems, multidimensional grids are of course in order. For the specific three-dimensional case of an atom−diatom exchange reaction considered in this work, a common choice for the set of the three internal coordinates is the two interatomic distances (r_1 and r_2) plus the angle (ϕ) formed by the corresponding bonds. The resulting three-dimensional grid is set up using two BL grids (as defined for the diatom case) for r_1 and r_2 and an angular grid for ϕ.

In the following, we shall propose an alternative way for configuration-space sampling based on bond-order (BO) variables rather than BL ones (Section 2.1). We shall then review the fitting/interpolation schemes that have been used in this work (Section 2.2) and give the relevant computational details (Section 2.3) before benchmarking the performances of the considered sampling and fitting schemes in Section 3.

2.1. Space-Reduced Bond-Order Grid Approach. On the basis of the "bond order" concept dating back to the times of Pauling,[54] BO variables are defined as the exponential of the weighed diatomic displacement

$$n = e^{-\beta(r-r_e)} \tag{1}$$

where β is a constant related to one or more diatomic force constants, r_e is the equilibrium diatomic distance, and r is the familiar atom−atom internuclear distance (or bond-length, BL, variable) of the diatom. As concisely pointed out by Laganà for the first time in a letter of 1991,[55] the appeal of BO variables for use in dynamics studies lies in the property of the BO space of having the origin at infinite internuclear distances and to confine the physical space inside the limiting value $e^{\beta r_e}$. A further property of BO variables following from their definition in eq 1 is that of confining the attractive and repulsive regions of a diatom configuration space in the (0,1) and (1, $e^{\beta r_e}$) range, respectively, with unity in BO space representing the equilibrium point. As a matter of fact, BO variables have been used in formulating polynomial representations of PESs[56,57] and rotating diatomic-like ones (like the rotating bond-order[55] and the largest-angle generalization of the rotating bond-order[58]). In addition, BO variables have been used for producing PES relaxed representations for evidencing process channels[49] and developing the related quantum reactive scattering formalism.[59,60]

As mentioned, in configuration-space sampling for PES fitting one usually excludes the strongly repulsive (dynamically inaccessible) regions and the near-asymptotic ones by introducing two boundary distances r_{min} and r_{max}. A balanced representation of the sampled attractive and repulsive region of the diatom configuration space can then be obtained in BO space by relaxing the condition that β is linked to the diatom spectroscopic properties and allow it to vary until a desired attractive over repulsive space ratio f is reached.[60]

$$f = \frac{1 - n_{min}}{n_{max} - 1} = \frac{1 - e^{-\beta(r_{max}-r_e)}}{e^{-\beta(r_{min}-r_e)} - 1} \tag{2}$$

We shall refer to the resulting BO variables as to space-reduced bond-order (SRBO) variables, in that once f has been fixed the same space relation between the attractive and repulsive regions of configuration space will hold for any considered diatom.[61]

Reasonable values of r_{min} and r_{max} tailored to a specific diatom can be obtained by modeling the diatom potential with a Morse function[62]

$$V(r) = D_e\left[1 - \exp\left(-\sqrt{\frac{k_e}{2D_e}}(r - r_e)\right)\right]^2 \tag{3}$$

DOI: 10.1021/acs.jpca.5b10018
J. Phys. Chem. A 2016, 120, 4683−4692

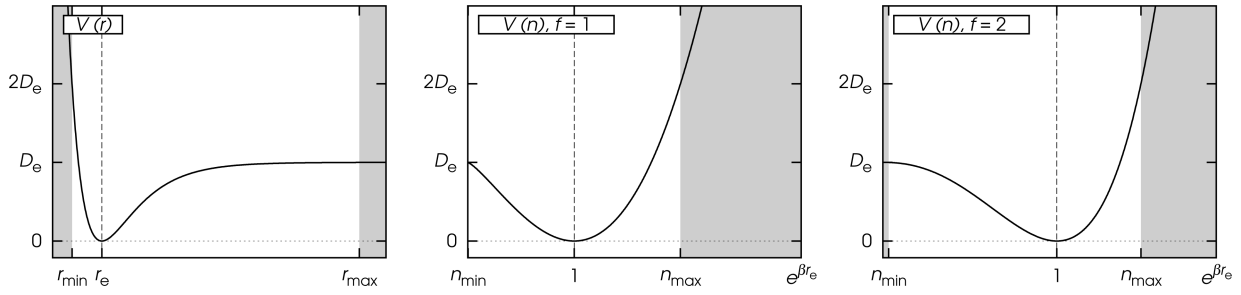

Figure 1. Morse potential for the H_2 diatom as a function of the bond-length variable r (left) and of two space-reduced bond-order (SRBO) variables $n = e^{-\beta(r-r_e)}$ yielding either $f = 1$ (center, $\beta = 0.813a_0^{-1}$) or $f = 2$ (right, $\beta = 0.464a_0^{-1}$). The Morse potential was modeled after FCI/VTZ data of Table 1 (Section 3), while r_{min} and r_{max} (n_{min} and n_{max}) were worked out by setting $V_{fact} = 2.0$ and $V_{thrs} = 0.001$.

whose parameters (the equilibrium distance r_e, the bond-dissociation energy D_e, and the force constant at equilibrium $k_e = d^2V/dr^2|_{r_e}$) are obtained by simple geometry optimization and by tuning the factors $V_{fact} = V(r_{min})/D_e$ and $V_{thrs} = [D_e - V(r_{max})]/D_e$ associated with the mentioned boundary values. Figure 1, for example, shows the Morse potential (modeled after FCI/VTZ data of Table 1, Section 3) for the H_2 diatom as a function of the bond-length variable r (left panel) and of two SRBO variables yielding either $f = 1$ (center panel, $\beta = 0.813a_0^{-1}$) or $f = 2$ (right panel, $\beta = 0.464a_0^{-1}$), where boundaries r_{min} and r_{max} (n_{min} and n_{max}) were chosen by setting $V_{fact} = 2.0$ and $V_{thrs} = 0.001$. In this way boundaries are obtained to the sampled configuration space that are linked to a diatom-specific physical model rather than being arbitrary (the white area in Figure 1 is limited on the left to the distance where the Morse potential is twice the dissociation energy and on the right to the distance where it has reached the dissociation energy within 1 ‰).

Table 1. Full-Configuration Interaction Values[a]

	H_2			H_3	
	r_e/a_0	D_e/E_H	$k_e/E_Ha_0^{-2}$	r_s/a_0	D_s/E_H
VDZ	1.438	0.1651	0.3662	1.7826	0.1488
VTZ	1.403	0.1727	0.3707	1.7576	0.1569
AVTZ	1.404	0.1730	0.3694	1.7601	0.1576
VQZ	1.402	0.1739	0.3697	1.7575	0.1584

[a]Include the equilibrium distance r_e, bond-dissociation energy D_e, and force constant at equilibrium k_e for H_2, plus the value r_s of the two interatomic distances at the H_3 collinear symmetric saddle-point and the dissociation energy D_s from the H_3 saddle point computed using VDZ, VTZ, AVTZ, and VQZ basis sets.

Once an optimal attractive over repulsive space ratio parameter f has been chosen and boundaries r_{min} and r_{max} have been set, the diatom configuration space can be conveniently sampled by a uniform grid on the segment of the resulting SRBO variable between n_{min} and n_{max}. The way SRBO grids have been generated in this paper is as follows:

1. fix the boundary values r_{min} and r_{max} in physical space (n_{min} and n_{max} in BO space) by setting V_{fact} and V_{thrs}
2. choose the couple (N_r, N_a) of grid points in the repulsive (r) and attractive (a) region, respectively, of the diatom configuration space (either physical or BO)
3. compute the SRBO mapping parameter β yielding $f = N_a/N_r$ from eq 2
4. set up a uniform grid of $N_r + N_a + 1$ (the added 1 accounts for the equilibrium geometry that is, obviously, neither attractive nor repulsive) points on the segment of n ranging from n_{min} to n_{max}.

This type of SRBO grids shall be referred to hereinafter as (N_r, N_a), like the seven-point (2, 4) shown in the right-hand-side panel of Figure 2. In that figure, the corresponding grid points in physical space are also shown in the left-hand-side panel. The advantages of an SRBO sampling over a BL one appear now from the same figure. The points of an SRBO grid are concentrated in the high-gradient region of the potential and, as already shown in ref 60, better sample the relevant configuration-space regions than the points of a uniform BL grid of the same size.

As mentioned, for a triatomic system a three-dimensional BL grid is usually set up using two grids in r_1 and r_2 plus an angular one in the already mentioned angle ϕ. Such grid can be replaced by an SRBO one for n_1 and n_2 while keeping the same angular grid for ϕ.

2.2. Fitting and Interpolation Schemes. Once a set of ab initio points has been generated, the next step is to fit them to (or interpolate them with) an analytic functional form. The analytic representation of the PES can be either local (see, for instance, Collins' modified Shepard[32,50,63−65] and Schatz's

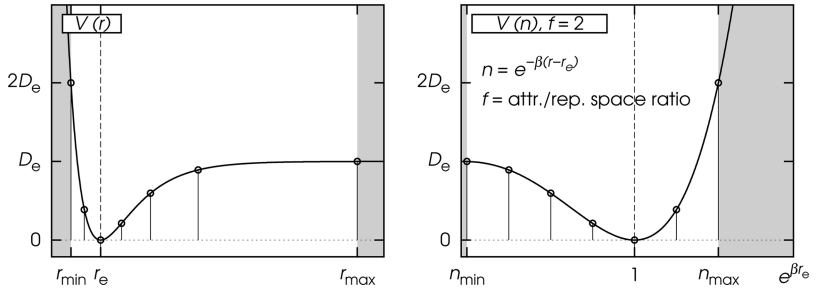

Figure 2. Points of a (2, 4) SRBO grid (see text for discussion) in (left) physical space and (right) BO space (see also Figure 1 and related caption).

DOI: 10.1021/acs.jpca.5b10018
J. Phys. Chem. A 2016, 120, 4683−4692

interpolant moving least-squares[66,67] schemes) or global (usually of the dumped-polynomial type). In local schemes, the fitted/interpolated value of the PES in a given point of configuration space depends on the values of the neighboring ab initio points, while in global schemes the fitted/interpolated value of the PES in a given point of configuration space depends on the values of the whole set of ab initio points available. The reader is referred to the reviews cited in the Introduction for a complete account of local and global fitting/interpolation schemes. In this paper we focus on the modified-Shepard[50] local interpolation and Aguado−Paniagua[51,52] global fitting (Sh and AP, respectively, hereinafter) that have been used in this work for both the one-dimensional and three-dimensional test cases.

In the modified-Shepard[50] local-interpolation scheme a many-body potential is written as a weighed sum of second-order Taylor expansions around a set of N_{Sh} ab initio energies

$$V(\boldsymbol{q}) = \sum_{i=1}^{N_{Sh}} w_i(\boldsymbol{q}) T_i(\boldsymbol{q}) \tag{4}$$

where $\boldsymbol{q}$ is the vector of the N_q internal coordinates (N_q = 1 for a diatom, N_q = 3 for a triatom), $w_i(\boldsymbol{q})$ are weight functions, and $T_i(\boldsymbol{q})$ are second-order Taylor expansions around the ith ab initio energy. These are given by

$$T_i(\boldsymbol{q}) = V_i + \sum_{\alpha=1}^{N_q} \Delta q_\alpha \left.\frac{\partial V}{\partial q_\alpha}\right|_i + \frac{1}{2!}\sum_{\alpha=1}^{N_q}\sum_{\beta=1}^{N_q} \Delta q_\alpha \Delta q_\beta \left.\frac{\partial^2 V}{\partial q_\alpha \partial q_\beta}\right|_i \tag{5}$$

where Δq_α is the difference between coordinate α of the desired $\boldsymbol{q}$ space point and coordinate α of the geometry of the ith ab initio energy. The following inverse-distance weighting is herein adopted

$$w_i = \frac{1}{d_i} \Big/ \sum_{j=1}^{N_{Sh}} w_j \tag{6}$$

where

$$d_i = \sqrt{\sum_{\alpha=1}^{N_q} (\Delta q_\alpha)^2} \tag{7}$$

As mentioned earlier the chosen internal coordinate for the diatom is the interatomic distance r, while the set of internal coordinates for the triatom are the two interatomic distances r_1 and r_2 plus the angle ϕ formed by the related bonds. Because of regularity in the grid definitions adopted in this work and previously described, the sum in eq 4 (which in the original scheme runs over the whole set of available data) is here extended only to the points "bracketing" the desired $\boldsymbol{q}$. N_{Sh} is therefore limited to 2 (left-hand-side and right-hand-side points) for the one-dimensional case and to 8 (those defining the parallelepiped containing space-point $\boldsymbol{q}$) for the three-dimensional case.

The AP global-fitting scheme is described in detail in refs 51 and 68, and computer programs for three- and four-body potential fitting have been published.[52,69,70]

Its main features as to the two- and three-body fitting used in this work are as follows. A diatomic (two-body) potential is given the functional form

$$V^{(2)}(r) = c_0 \frac{e^{-\alpha r}}{r} + \sum_{i=1}^{I} c_i (r e^{-\gamma^{(2)} r})^i \tag{8}$$

where α, c_0, and $\gamma^{(2)} > 0$ and the linear c_0, c_1, ..., c_I and nonlinear α and $\gamma^{(2)}$ parameters are determined by fitting a set of ab initio values of the diatomic potential energy. Following a many-body expansion[71] and omitting for clarity the constant one-body terms, a three-body potential is written as a sum of three two-body and one three-body terms

$$V(r_1, r_2, r_3) = V_1^{(2)}(r_1) + V_2^{(2)}(r_2) + V_3^{(2)}(r_3) + V^{(3)}(r_1, r_2, r_3) \tag{9}$$

where subscripts 1, 2, and 3 label the three possible diatoms and the three-body term is given by

$$V^{(3)}(r_1, r_2, r_3) = \sum_{ijk}^{M} d_{ijk} (r_1 e^{-\gamma_1^{(3)} r_1})^i (r_2 e^{-\gamma_2^{(3)} r_2})^j (r_3 e^{-\gamma_3^{(3)} r_3})^k \tag{10}$$

with $i + j + k \neq i \neq j \neq k$ and $i + j + k \leq M$. Linear d_{ijk} and nonlinear $\gamma_1^{(3)}$, $\gamma_2^{(3)}$, and $\gamma_3^{(3)}$ parameters in the equation above are determined by fitting the ab initio values of the potential energy of triatomic system minus the diatomic potentials at the corresponding internuclear distances.

2.3. Computational Details. Ab initio calculations were performed at full configuration-interaction (FCI) level of theory with the MOLPRO package[72] version 2010.1 using Dunning's correlation-consistent basis sets cc-pVDZ, cc-pVTZ, aug-cc-pVTZ, and cc-pVQZ (hereafter VDZ, VTZ, AVTZ, and VQZ, respectively).[73] Energy partial derivatives required in eq 5 were computed numerically by two-point central finite-difference scheme using displacements $0.01a_0$ for distances and 1.0° for angles.

The AP fit was performed using the GFIT3C program,[52] employing a sixth-degree polynomial fit for the two-body term and a ninth-degree polynomial fit for the three-body term. The correct permutational symmetry was ensured by setting input parameter `INDICE` = 1 (specifying an A_3 system as opposed to AB_2 or ABC, with A, B, and C labeling the three atoms). The Sh interpolation was performed using ad hoc in-house written software.

Reactive scattering calculations on the H + H_2→ H_2 + H atom-exchange reaction for total angular momentum J = 0 and total-energy range of 0.4−1.4 eV were performed within a TI hyperspherical-coordinate formalism as implemented in the ABC program[74] by setting input parameters `emax` = 2.4 eV (maximum internal energy in any channel), `jmax` = 50 (maximum rotational quantum number in any channel), `rmax` = 12.0a_0 (maximum hyperradius), and `mtr` = 150 (number of log-derivative propagation sectors).

A computer program for generating SRBO grids starting from input parameters r_e, D_e, k_e, V_{fact}, V_{thrs}, and the desired couple (N_r, N_a) is made available.[75]

3. RESULTS

As already mentioned, the H_2 and H_3 prototype systems were chosen for the purpose of assessing the performances of an SRBO-based configuration-space sampling for PES fitting of few-atom reactive system. It is worth here pointing out again that, accordingly, proposing a new functional formulation of the H_2 bond-dissociation curve and H_3 reactive PES is not the scope of the present paper. Published high-accuracy PESs for H_3 are LSTH[76−79] (based on 287 ab initio energy points),

DOI: 10.1021/acs.jpca.5b10018
J. Phys. Chem. A 2016, 120, 4683−4692

DMBE[80] (based on 316 points), BKMP[81] (based on 772 points), BKMP2[82] (based on 8701 points), and the exact quantum Monte Carlo (EQMC)-based one[83] (based on ~76 000 points).

As a compromise between accuracy and computational cost, a VTZ basis set was chosen for computing the required ab initio energies. For sake of comparison, the H_2 equilibrium distance r_e, bond-dissociation energy D_e (given as minus the difference of the energy at equilibrium and that at $r = 30a_0$), the force constant at equilibrium k_e plus the value r_s of the two interatomic distances at the H_3 collinear symmetric saddle, and the dissociation energy D_s from the H_3 saddle point (given as minus the difference of the energy at the saddle point and that at a collinear configuration with two interatomic distances set to $30a_0$) computed using VDZ, VTZ, AVTZ, and VQZ basis sets are given in Table 1 (see ref 84 for a more complete account of basis-set accuracy on these quantities). VTZ calculations, that as mentioned were selected throughout the paper, yield a D_e for H_2 of 4.70 eV ($0.1651E_H$) and a classical-barrier height for the $H + H_2 \rightarrow H_2 + H$ reaction $-(D_s - D_e)$ of 0.43 eV ($0.0158E_H$).

In the following subsections a cross comparison is performed of the two (SRBO and BL) sampling schemes combined with the two (AP and Sh) fitting/interpolation schemes outlined in Section 2. We shall refer to the resulting four fit schemes as to SRBO-AP, SRBO-Sh, BL-AP, and BL-Sh. For both the SRBO and BL sampling, factors V_{fact} and V_{thrs} were set to 2.0 and 0.001, respectively. Using the FCI/VTZ data of Table 1 for Morse modeling, this choice leads to values of r_{min} and r_{max} of 0.553 and $8.740a_0$, respectively. The various grids that were set up for the considered one- and three- dimensional problems will be discussed in the relevant paragraphs of Section 3, where results are illustrated.

The quality of each of the SRBO-AP, SRBO-Sh, BL-AP, or BL-Sh fits was evaluated by computing the root-mean-square error (RMSE) of the resulting fitted/interpolated potential with respect to a reference set of ab initio values ("reference set" hereafter) computed on a grid finer than that used for configuration-space sampling in generating the fitted/interpolated PESs. The reference set for the diatom H_2 was computed on an $N = 97$ uniform BL grid defined on the same already discussed r_{min} and r_{max}. That for the triatom H_3 was computed on a 25×25 two-dimensional uniform BL grid with same r_{min} and r_{max} as above and an angular grid ranging from 180° to 90° in steps of 15°.

The following issues were addressed:

(i) which is the optimal attractive over repulsive space ratio f for a diatom configuration-space sampling?
(ii) how do the considered sampling/fitting schemes compare in the one-dimension fit of a diatom potential curve?
(iii) how do the considered sampling/fitting schemes compare in the three-dimension fit of a three-atoms reactive PES?
(iv) how does configuration-space sampling affect the reproduction of dynamical properties?

3.1. One-Dimensional H_2. (i) A first point to address is the determination of the optimal attractive over repulsive space-ratio parameter f for a diatom configuration-space sampling. We selected for that purpose a trial number of total grid points $N = 13$ and tested the fitting quality, using both the AP and the Sh schemes, for several grids featuring a different distribution (resulting in a different value of f) of points among the repulsive and attractive regions. Among the possibilities offered by a total number of grid points $N = 13$, the following grids were selected: (8,4), (6,6), (4,8), (3,9), (2,10) yielding f values of 0.5, 1.0, 2.0, 3.0, and 5.0, respectively. Results in terms of RMSE values with respect to the reference set are summarized in Table 2 and plotted in Figure 3.

Table 2. RMSE with Respect to the Reference Set (see the introductory note to Section 3) of Both an AP and Sh Fit to a Set of $N = 13$ H_2 Energies[a]

		RMSE, eV	
f	(N_r, N_a)	SRBO-AP	SRBO-Sh
0.5	(8,4)	0.025	0.725
1.0	(6,6)	0.008	0.119
2.0	(4,8)	0.004	0.052
3.0	(3,9)	0.006	0.093
5.0	(2,10)	0.067	0.190

[a]Computed at the points of several uniform space-reduced bond-order (SRBO) grids (see Section 2.1) as a function of the attractive over repulsive space ratio f. The RMSEs using a corresponding $N = 13$ uniform bond-length (BL) grid are 0.149 and 0.336 eV for an AP and Sh fit, respectively.

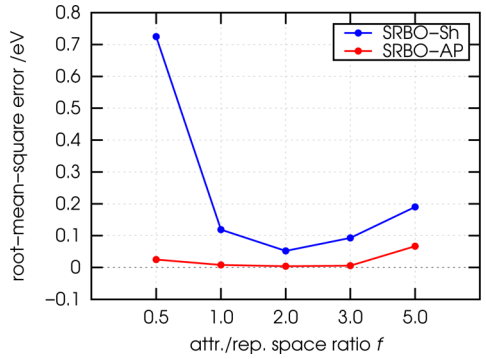

Figure 3. Plot of the RMSEs given in Table 2 for the one-dimensional H_2 test case as a function of the attractive over repulsive space ratio f.

As apparent from the figure, both the SRBO-AP (red) and the SRBO-Sh (blue) curves show a U-shape trend indicating that at the considered extrema the configuration-space sampling is unbalanced either in the repulsive or in the attractive region. For both the AP and Sh fit, the optimal value of f turns out to be 2, whereby the number of points located in the attractive region is twice that of the points located in the repulsive region.

A few additional comments are in order for Figure 3. The first is that, for the specific case of $N = 13$, an Sh fit performs in general worse than an AP one (we will explore better this point in the next paragraph). A second comment is that using the Sh scheme the largest error is associated with the oversampling of the repulsive region (0.725 eV for the (8,4) grid), while using the AP scheme the largest error is associated with the oversampling of the attractive region (0.067 for the (2,10) grid). Moreover, by error-comparison of the (8,4) versus the (4,8) fits, both the AP (0.025 vs 0.004 eV) and the Sh (0.725 vs 0.052 eV) fits show to be more sensitive to a richer sampling of the attractive region than of the repulsive one. A last note anticipating the next coming discussion on the suitability of an SRBO versus BL sampling deserves the comparison of previous results with the RMSEs computed on a corresponding (equally

DOI: 10.1021/acs.jpca.5b10018
J. Phys. Chem. A 2016, 120, 4683−4692

sized) N = 13 BL grid that gives 0.149 eV for the AP fit and 0.336 eV for the Sh fit. This means that so far, except for the case of the (8,4) SRBO-Sh fit, an SRBO sampling performs always better than a BL one.

(ii) As just anticipated, the second point to address is the performance comparison of the SRBO sampling with that of the BL one for both the AP and Sh fits. We selected for that purpose an initial very coarse grid (2,4) (namely, the already commented 7-point grid shown in the Table of Contents graphics) and then built successive grids by keeping f = 2 and adding one point in the repulsive region and two points in the attractive region until reaching a very dense grid of total number of points N = 49. RMSEs for the fits based on these grids are listed for comparison in Table 3. The same data are plotted as a function of the total number of grid points N in Figure 4 as solid red curve for SRBO-AP, solid blue curve for SRBO-Sh, dashed red curve for BL-AP, and dashed blue curve for BL-Sh.

Table 3. RMSEs of Both an AP and Sh Fit to a Set of N H_2 Energies[a]

		RMSE, eV			
N	(N_r, N_a)	SRBO-AP	SRBO-Sh	BL-AP	BL-Sh
7	(2,4)	0.117	0.189	0.139	1.667
10	(3,6)	0.007	0.091	0.166	0.468
13	(4,8)	0.004	0.052	0.149	0.336
16	(5,10)	0.007	0.035	0.064	0.270
19	(6,12)	0.003	0.024	0.122	0.216
22	(7,14)	0.007	0.016	0.053	0.175
25	(8,16)	0.007	0.009	0.018	0.143
28	(9,18)	0.007	0.005	0.009	0.118
31	(10,20)	0.007	0.008	0.007	0.099
34	(11,22)	0.007	0.007	0.007	0.084
37	(12,24)	0.007	0.006	0.006	0.072
40	(13,26)	0.007	0.005	0.006	0.062
43	(14,28)	0.007	0.004	0.006	0.054
46	(15,30)	0.007	0.004	0.006	0.047
49	(16,32)	0.007	0.003	0.006	0.041

[a]Computed at the points of uniform SRBO grids of different grain from very coarse (7-point) to very dense (49-point) and featuring an attractive over repulsive space ratio f = 2. RMSEs for the corresponding uniform BL grids are also reported.

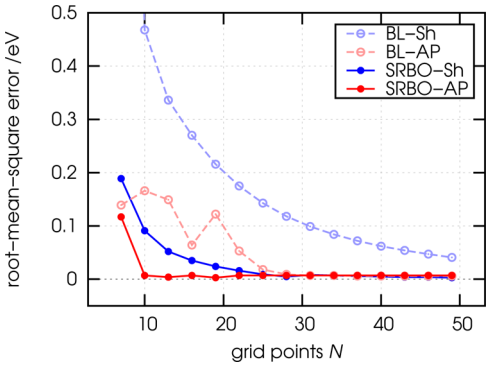

Figure 4. Plot of the RMSEs given in Table 3 for the one-dimensional H_2 testcase as a function of the number of grid points N.

As apparent, an SRBO sampling (solid curves) performs always better than a BL one (dashed curves) making the fitted PES converge faster to the ab initio-computed one with the number of grid points N using either the AP or Sh fitting scheme. The best performances are recorded for the SRBO-AP fit, which converges to an error smaller than 0.01 eV already at N = 10. The same result is achieved by the SRBO-Sh fit at N = 25, by the BL-AP fit only at N = 28 and never, in the considered range of N, by the BL-Sh fit.

At this point a comment is due on the comparison between the AP and Sh fitting schemes themselves. The functional formulation of the AP method guarantees a good outcome even for very small grids, where instead, in Sh fits, the points are too distant to allow for good convergence of the Taylor expansion in the regions amid two points. This can lead to a qualitatively wrong shape of the potential, as shown in Figure 5 for an Sh fit on N = 13 SRBO and BL grids. In fact, while the points of an SRBO sampling are well-distributed between the attractive and repulsive regions of the H_2 configuration space, those of a BL sampling are mainly concentrated in the attractive tail of the potential leading to an erroneous fit in the near-equilibrium and repulsive region.

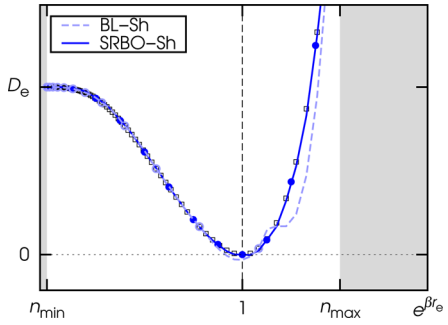

Figure 5. Sh fit of the H_2 potential using both a (4,8) SRBO sampling grid and an N = 13 corresponding BL grid as a function of an f = 2 SRBO variable. Small empty squares are the reference FCI/VTZ data.

However, the rigidity imposed by the functional form in the AP fit turns out to be a limiting factor to the accuracy when increasing N. In fact, while both the SRBO-AP and BL-AP fits quickly reach their (limited) best performances, the errors of an Sh fit are seen to tend to zero with increasing N. In other words, while the AP fit accuracy is limited by the adopted functional form, the Sh one can be refined at pleasure just by using denser grids. For the same reason, an SRBO sampling outperforms a BL sampling more when using Sh fits than AP ones, where the fit is somehow "aided" by the fixed functional form.

3.2. Three-Dimensional H_3. (iii) As is known, relying on an as small as possible set of data is increasingly more important in higher dimensionality problems. As mentioned before, for the three-body configuration-space sampling of H_3 three-dimensional grids in the internal coordinates r_1 and r_2 (two bond distances) and ϕ (the angle formed by the related bonds) were adopted. An angular grid of five values ranging from 180° (collinear configuration) to 60° in steps of 30° was set up. SRBO (3,6), (4,8), (5,10), and (6,12) grids were considered for each of the r_1 and r_2 coordinates, setting the attractive over repulsive space ratio parameter f equal to 2. The corresponding (equally sized) 10-, 13-, 16-, and 19-point BL grids were considered, too. Because of the symmetry of the system, for each angle only $\frac{1}{2} \times (N_r + N_a + 1) \times [(N_r + N_a + 1) + 1]$ rather than

DOI: 10.1021/acs.jpca.5b10018
J. Phys. Chem. A 2016, 120, 4683−4692

$(N_r + N_a + 1)^2$ grid points were computed (only the points for which $r_2 \leq r_1$). The saddle point reported in Table 1 was added to the ensemble of points. The corresponding final three-dimensional grids are made of $N = \frac{(N_r + N_a + 1) \times [(N_r + N_a + 1) + 1]}{2} \times 5 + 1$, which makes a total of 276, 456, 681, and 951 points, respectively, for the four SRBO (and corresponding BL) one-dimensional grids described above. For illustrative purposes, the points of the fixed angle (ϕ = 180°) two-dimensional SRBO (3,6) grid in r_1 and r_2 are depicted in Figure 6.

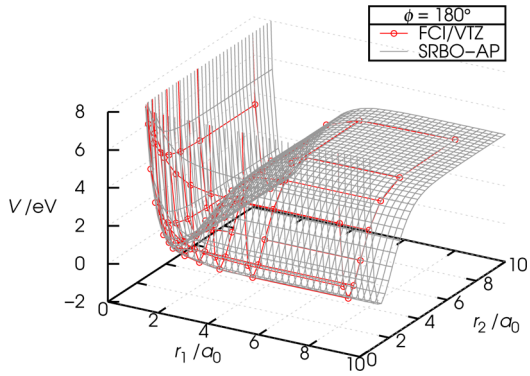

Figure 6. Scheme of a fixed angle (ϕ = 180°) two-dimensional SRBO (3,6) grid in r_1 and r_2 used for the three-dimensional H_3 test case. Computed FCI/VTZ points together with the SRBO-AP fitted surface are also shown. The energy zero is set to the bottom of the reactant valley.

RMSE values for the four combinations SRBO-AP, SRBO-Sh, BL-AP, and BL-Sh and the considered grids are listed in Table 4. Except for the BL-Sh case whose data are out of the represented range, the same data are plotted in Figure 7 as a function of the total number of grid points N using the same line type and colors as in Figure 4. Note that, as a consequence of the higher complexity of the three-dimensional problem, RMSEs are ∼1 order of magnitude higher than those of the corresponding one-dimensional fit of the H_2 potential previously discussed.

Table 4. RMSEs of Both an AP and Sh Fit to a Set of N = 276, 456, 681, and 951 H_3 Energies Computed at the Points of SRBO and BL Grids

		RMSE, eV			
		SRBO		BL	
N	r grid	AP	Sh	AP	Sh
276	(3,6)	0.029	0.123	1.455	11.636
456	(4,8)	0.026	0.060	0.264	3.636
681	(5,10)	0.027	0.021	0.144	2.982
951	(6,12)	0.025	0.016	0.077	2.407

The same conclusions drawn from the analysis of the one-dimensional H_2 problem appear to apply here and to be even amplified. An AP fit on an SRBO sampling reaches a convergence to better than 0.03 eV already with the first (coarsest) N = 276 grid. An Sh fit on the same data performs slightly worse for the first two grids but goes below the AP error limit for the last two (finer) grids. This confirms the outcome of the analysis performed in Section 3.1, where the AP fit was seen to guarantee a better outcome for small grids

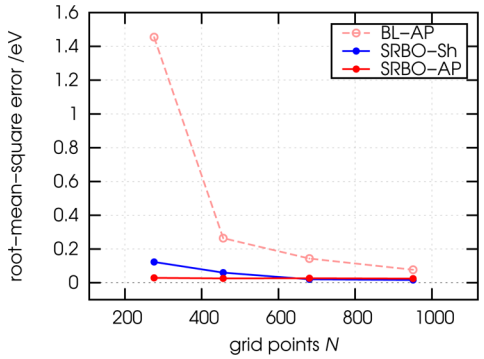

Figure 7. Plot of the RMSEs given in Table 4 for the three-dimensional H_3 test case as a function of the number of grid points N. Note that BL-Sh data are out of the represented range.

thanks to its fixed functional form, whereas the Sh fit was seen to perform better, tending to the exact PES, for larger N. At the same time BL sampling provides much worse fits, with the BL-AP best error being three times larger than that of the SRBO-AP fit and the BL-Sh fit yielding qualitatively worst PESs.

(iv) In this final paragraph we measure the quality of the above obtained PESs via a comparison of the outcomes of quantum dynamics calculations. We select for that purpose the AP fitting scheme and focus on the grain of the sampling grids discussed at point (iii) (from the coarsest, N = 276, through N = 456, 681, to the finest, N = 951). Cumulative reaction probabilities (CRPs, summing over all reactant v,j and product v',j' rovibrational states) for the H + $H_2(v, j)$ → $H_2(v', j')$ + H atom-exchange reaction computed on several PESs at total angular momentum J = 0 (using the TI method as described in Section 2.3) are plotted in Figure 8 as a function of the total

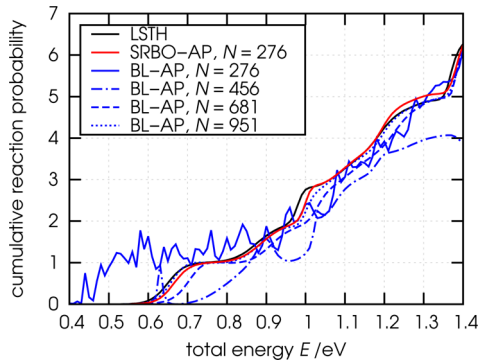

Figure 8. CRPs computed on PESs fitting a set of N = 276, 456, 681, and 951 ab initio energies as a function of the total energy E. CRPs computed on the popular LSTH PES are also shown for reference.

(collision plus internal) scattering energy E. CRPs computed on the popular LSTH PES (solid black curve) are also shown for reference. Red color is used for SRBO PESs and blue color for BL ones. Colored solid, dashed-dotted, dashed, and dotted lines refer to PESs built out of the N = 276, 456, 681, and 951 sampling grids, respectively.

In line with the RMSE results discussed at point (iii), CRPs computed on the SRBO-AP PESs are already converged for the coarsest N = 276 sampling grid. Accordingly, in Figure 8 only the SRBO-AP CRPs for N = 276 (solid red line) are reported, while the superimposing N = 456, 681, and 951 cruves are omitted for clarity. Remarkably, on the other hand, fitted PESs based on a BL fitting provide CRPs (blue lines) of poorer

DOI: 10.1021/acs.jpca.5b10018
J. Phys. Chem. A 2016, 120, 4683−4692

quality with convergence still incomplete even with the largest grid. Finally, the suitability of the obtained SRBO-AP PES is confirmed by the smoothness and structure of the computed CRPs that well compare with those computed on the popular LSTH surface. CRPs computed on the LSTH PES, in fact, are, as expected, slightly shifted toward lower energies as a consequence of the featured slightly lower barrier height[76−79] (0.42 vs 0.43 eV) along the minimum energy path (which turns into a lower threshold to reactivity) while reproducing the overall smooth shape.

4. CONCLUSIONS AND PERSPECTIVES

In this paper an automated scheme for optimal configuration-space sampling in potential-energy evaluation and fitting for few-atom reactive systems is proposed for incorporation of the related modules into the grid-empowered molecular simulator GEMS. The scheme is based on a space-reduced formulation of the so-called bond-order variables allowing for a balanced representation of the attractive and repulsive regions of a diatom configuration space. The related SRBO variables are easily constructed from the values of the diatom equilibrium distance r_e, bond-dissociation energy D_e, and force constant at equilibrium k_e according to a desired value of the parameter f, the ratio between the attractive and repulsive range of the diatom configuration space. The diatom configuration space can then be conveniently sampled by uniform grids in SRBO variables, which are used as building blocks for multidimensional grids in higher-dimensionality problems.

The suitability of uniform SRBO grids in sampling configuration space for PES fitting was first assessed for the prototype one-dimensional problem of the H_2 bond-dissociation curve versus the more conventional sampling based on uniform grids in interatomic distances (or BL variables). Both a local-interpolation (modified Shepard) and a global-fitting (Aguado−Paniagua) scheme were considered for that purpose. Benchmark calculations show that optimal SRBO performances are reached when β is set such as to yield an f value equal to 2, whereby the number of points sampling the attractive region is twice the number of points sampling the repulsive one. SRBO sampling is then seen in general to outperform BL sampling in converging the fitted PES to the computed ab initio one with the number of grid points, independently of the adopted fitting/interpolation scheme. Further benchmarks were repeated for the three-dimensional problem of the reactive PES of the H_3 system suitable for studying the atom-exchange reaction $H + H_2 \rightarrow H_2 + H$. Although the SRBO approach itself does not improve, over other grid-based approaches, the scaling of the required number of sampling points with increasing dimensionality of the problem, calculations on the considered three-dimensional case (including time-independent quantum dynamics) fully confirm the results obtained for the one-dimensional test indicating that the proposed scheme, compared to a conventional BL-based one, offers a way of selecting a reduced most informative set of configurations.

The f ratio is shown to be a useful tool for improving various fitting techniques based on exponentially scaled distances (see, e.g., the works by Xie and Bowman[85] and by Zhu and Yarkony[86]). In these approaches, in fact, no clear procedure seems to have been established to determine the exponential scaling factor, and one might consider grounding this choice on the f ratio rather than on trial and error procedures or even an arbitrary choice. A twofold configuration-space partition might also turn useful in more complex scenarios in which multiple minima occur in two-body interaction curves, where one might pick the deepest minimum or the relative maximum between two minima as the divide-point between two areas and then suitably adjust the related f ratio.

The conceptual advantage of the proposed SRBO configuration-space sampling was found to lie in the fact that the resulting choice of geometries has built-in a force-based metric rather than a purely spatial one as in BL sampling. Of course, the issuing of some caveats is in order. First, SRBO sampling focuses on the strong interaction region, whereas for some processes like the non-reactive and reorientation collisions, an accurate modeling of the long-range interaction regions is mandatory (see, e.g., ref 87). Then, specific features of reactive PESs such as wells or saddles are known to require specific attention, and a rectangular domain of the SRBO grid might be inappropriate. This has called our attention to PES-channel-related variables adapting the grids of BO points to auxiliary variables linked to minimum energy paths.[55,58,88] Moreover, the SRBO approach may be usefully combined with the previoulsy quoted approaches seeking PES refinement either via dynamical sampling with classical trajectories or through successive-degree fitting, as in the most recent scheme by the Dawes group.[34]

Extensions of the SRBO approach to higher dimensionality problems with SRBO variables being employed for the breaking and forming bonds mixed with other internal coordinates are being pursued, while applications to compute for the first time the ground-state PES of the system C_2H^+ to model the reactive process $C + CH^+ \rightarrow C_2^+ + H$ of interest in interstellar chemistry will be soon published.[53]

AUTHOR INFORMATION

Corresponding Author

*E-mail: srampino@thch.unipg.it. Phone: +39 075 5855532. Fax: +39 075 5855606.

Notes

The authors declare no competing financial interest.

ACKNOWLEDGMENTS

The author is grateful to Prof. A. Laganà for a critical reading of the manuscript and for his constant support over the last ten years in matters of science and beyond.

REFERENCES

(1) Balakrishnan, N.; Kalyanaraman, C.; Sathyamurthy, N. Time-dependent quantum mechanical approach to reactive scattering and related processes. *Phys. Rep.* **1997**, *280*, 79−144.

(2) Althorpe, S. C. Quantum wavepacket method for state-to-state reactive cross sections. *J. Chem. Phys.* **2001**, *114*, 1601−1616.

(3) Balint-Kurti, G. Wavepacket quantum dynamics. *Theor. Chem. Acc.* **2010**, *127*, 1−17.

(4) Crawford, J.; Parker, G. A. State-to-state three-atom time-dependent reactive scattering in hyperspherical coordinates. *J. Chem. Phys.* **2013**, *138*, 054313.

(5) Pack, R. T.; Parker, G. A. Quantum reactive scattering in three dimensions using hyperspherical (APH) coordinates. Theory. *J. Chem. Phys.* **1987**, *87*, 3888−3921.

(6) Miller, W. H. Recent Advances in Quantum Mechanical Reactive Scattering Theory, Including Comparison of Recent Experiments with Rigorous Calculations of State-to-State Cross Sections for the H/D + H_2 →H_2/HD + H Reactions. *Annu. Rev. Phys. Chem.* **1990**, *41*, 245−281.

(7) Jaquet, R. Quantum reactive scattering: the time-independent approach. I. Principles and early developments. *Lect. Notes Chem.* **2001**, *77*, 17−82.

DOI: 10.1021/acs.jpca.5b10018
J. Phys. Chem. A 2016, 120, 4683−4692

(8) Jaquet, R. Quantum reactive scattering: The time independent approach. II Current methods and developments. *Lect. Notes Chem.* **2001**, *77*, 83−126.
(9) Nyman, G.; Yu, H.-G. Quantum theory of bimolecular chemical reactions. *Rep. Prog. Phys.* **2000**, *63*, 1001−1059.
(10) Casavecchia, P. Chemical reaction dynamics with molecular beams. *Rep. Prog. Phys.* **2000**, *63*, 355−414.
(11) Schatz, G. C.; Kuppermann, A. Quantum mechanical reactive scattering for three-dimensional atom plus diatom systems. I. Theory. *J. Chem. Phys.* **1976**, *65*, 4642−4667.
(12) Schatz, G. C.; Kuppermann, A. Quantum mechanical reactive scattering for three-dimensional atom plus diatom systems. II. Accurate cross sections for H + H_2. *J. Chem. Phys.* **1976**, *65*, 4668−4692.
(13) Bowman, J. M.; Schatz, G. C. Theoretical Studies of Polyatomic Bimolecular Reaction Dynamics. *Annu. Rev. Phys. Chem.* **1995**, *46*, 169−196.
(14) Althorpe, S. C.; Clary, D. C. Quantum Scattering Calculations on chemical reactions. *Annu. Rev. Phys. Chem.* **2003**, *54*, 493−529.
(15) Beck, M. H.; Jäckle, A.; Worth, G. A.; Meyer, H.-D. The multiconfiguration time-dependent Hartree (MCTDH) method: a highly efficient algorithm for propagating wavepackets. *Phys. Rep.* **2000**, *324*, 1−105.
(16) Helgaker, T.; Uggerud, E.; Jensen, H. J. A. Integration of the classical equations of motion on ab initio molecular potential energy surfaces using gradients and Hessians: application to translational energy release upon fragmentation. *Chem. Phys. Lett.* **1990**, *173*, 145−150.
(17) Chen, W.; Hase, W. L.; Schlegel, H. Ab initio classical trajectory study of H_2CO →H_2 + CO dissociation. *Chem. Phys. Lett.* **1994**, *228*, 436−442.
(18) Steckler, R.; Thurman, G. M.; Watts, J. D.; Bartlett, R. J. Ab initio direct dynamics study of OH + HCl →Cl + H_2O. *J. Chem. Phys.* **1997**, *106*, 3926−3933.
(19) London, F. Quantenmechanische Deutung Des Vorgangs Der Aktivierung. *Z. Elektrochem. Angew. Phys. Chem.* **1929**, *35*, 552−555.
(20) Eyring, H.; Polanyi, M. Über einfache Gasreaktionen. *Z. Phys. Chem., Abt. B* **1931**, *12*, 279−311.
(21) Sato, S. On a New Method of Drawing the Potential Energy Surface. *J. Chem. Phys.* **1955**, *23*, 592−593.
(22) Sato, S. Potential Energy Surface of the System of Three Atoms. *J. Chem. Phys.* **1955**, *23*, 2465−2466.
(23) Sathyamurthy, N. Computational fitting of ab initio potential energy surfaces. *Comput. Phys. Rep.* **1985**, *3*, 1−69.
(24) Truhlar, D. G.; Steckler, R.; Gordon, M. S. Potential energy surfaces for polyatomic reaction dynamics. *Chem. Rev.* **1987**, *87*, 217−236.
(25) Schatz, G. C. The analytical representation of electronic potential-energy surfaces. *Rev. Mod. Phys.* **1989**, *61*, 669−688.
(26) Schatz, G. Fitting Potential Energy Surfaces. *Lect. Notes Chem.* **2000**, *75*, 15−32.
(27) Varandas, A. J. C. Intermolecular and Intramolecular Potentials: Topographical Aspects, Calculation, and Functional Representation via A Double Many-Body Expansion Method. *Adv. Chem. Phys.* **1988**, *74*, 255−338.
(28) Hollebeek, T.; Ho, T.-S.; Rabitz, H. Constructing Multidimensional Molecular Potential Energy Surfaces from Ab Initio Data. *Annu. Rev. Phys. Chem.* **1999**, *50*, 537−570.
(29) Jaquet, R. Interpolation and fitting of potential energy surfaces: Concepts, recipes and applications. *Lect. Notes Chem.* **1999**, *71*, 97−175.
(30) Paukku, Y.; Yang, K. R.; Varga, Z.; Truhlar, D. G. Global ab initio ground-state potential energy surface of N_4. *J. Chem. Phys.* **2013**, *139*, 044309.
(31) Paukku, Y.; Yang, K. R.; Varga, Z.; Truhlar, D. G. Erratum: "Global ab initio ground-state potential energy surface of N_4" [J. CHEM. PHYS. 139, 044309 (2013)]. *J. Chem. Phys.* **2014**, *140*, 019903.
(32) Ischtwan, J.; Collins, M. A. Molecular potential energy surfaces by interpolation. *J. Chem. Phys.* **1994**, *100*, 8080−8088.
(33) Ishida, T.; Schatz, G. C. Automatic potential energy surface generation directly from ab initio calculations using Shepard interpolation: A test calculation for the H_2 + H system. *J. Chem. Phys.* **1997**, *107*, 3558−3568.
(34) Majumder, M.; Ndengue, S. A.; Dawes, R. Automated construction of potential energy surfaces. *Mol. Phys.* **2015**, 1.
(35) Laganà, A.; Costantini, A.; Gervasi, O.; Faginas Lago, N.; Manuali, C.; Rampino, S. COMPCHEM: Progress Towards GEMS a Grid Empowered Molecular Simulator and Beyond. *J. Grid Comput.* **2010**, *8*, 571−586.
(36) Rampino, S. Workflows and data models for atom diatom quantum reactive scattering calculations on the Grid. Ph.D. Thesis, Università degli Studi di Perugia, 2011.
(37) Manuali, C.; Laganà, A.; Rampino, S. GriF: A Grid framework for a Web Service approach to reactive scattering. *Comput. Phys. Commun.* **2010**, *181*, 1179−1185.
(38) Rampino, S.; Faginas Lago, N.; Laganà, A.; Huarte-Larrañaga, F. An extension of the grid empowered molecular simulator to quantum reactive scattering. *J. Comput. Chem.* **2012**, *33*, 708−714.
(39) Rampino, S.; Skouteris, D.; Laganà, A.; Garcia, E. A Comparison of the Isotope Effect for the N + N_2 Reaction Calculated on Two Potential Energy Surfaces. *Lect. Notes Comput. Sci.* **2008**, *5072*, 1081−1093.
(40) Laganà, A.; Faginas Lago, N.; Rampino, S.; Huarte Larrañaga, F.; García, E. Thermal rate coefficients in collinear versus bent transition state reactions: the N + N_2 case study. *Phys. Scr.* **2008**, *78*, 058116.
(41) Rampino, S.; Pirani, F.; Garcia, E.; Laganà, A. A study of the impact of long range interactions on the reactivity of N + N_2 using the Grid Empowered Molecular Simulator GEMS. *Int. J. Grid Web Services* **2010**, *6*, 196−212.
(42) Laganà, A.; Rampino, S. A Grid Empowered Virtual Versus Real Experiment for the Barrierless Li + FH →LiF + H Reaction. *Lect. Notes Comput. Sci.* **2014**, *8579*, 571−584.
(43) Rossi, E.; Evangelisti, S.; Laganà, A.; Monari, A.; Rampino, S.; Verdicchio, M.; Baldridge, K. K.; Bendazzoli, G. L.; Borini, S.; Cimiraglia, R.; et al. Code interoperability and standard data formats in quantum chemistry and quantum dynamics: The Q5/D5Cost data model. *J. Comput. Chem.* **2014**, *35*, 611−621.
(44) Rampino, S.; Monari, A.; Rossi, E.; Evangelisti, S.; Laganà, A. A priori modeling of chemical reactions on computational grid platforms: Workflows and data models. *Chem. Phys.* **2012**, *398*, 192−198.
(45) The European Grid Infrastructure. http://www.egi.eu/, Accessed: October 9, 2015.
(46) Rampino, S.; Skouteris, D.; Laganà, A.; García, E.; Saracibar, A. A comparison of the quantum state-specific efficiency of N + N_2 reaction computed on different potential energy surfaces. *Phys. Chem. Chem. Phys.* **2009**, *11*, 1752−1757.
(47) Rampino, S.; Garcia, E.; Pirani, F.; Laganà, A. Accurate Quantum Dynamics on Grid Platforms: Some Effects of Long Range Interactions on the Reactivity of N + N_2. *Lect. Notes Comput. Sci.* **2010**, *6019*, 1−12.
(48) Rampino, S.; Skouteris, D.; Laganà, A. The O + O_2 reaction: quantum detailed probabilities and thermal rate coefficients. *Theor. Chem. Acc.* **2009**, *123*, 249−256.
(49) Rampino, S.; Skouteris, D.; Laganà, A. Microscopic branching processes: The O + O_2 reaction and its relaxed potential representations. *Int. J. Quantum Chem.* **2010**, *110*, 358−367.
(50) Shepard, D. A Two-Dimensional Interpolation Function for Irregularly-Spaced Data. In *Proceedings of the 1968 23rd ACM National Conference;* New York, NY; ACM Publications, 1968; pp 517−524.
(51) Aguado, A.; Paniagua, M. A new functional form to obtain analytical potentials of triatomic molecules. *J. Chem. Phys.* **1992**, *96*, 1265−1275.
(52) Aguado, A.; Tablero, C.; Paniagua, M. Global fit of ab initio potential energy surfaces I.Triatomic systems. *Comput. Phys. Commun.* **1998**, *108*, 259−266.

DOI: 10.1021/acs.jpca.5b10018
J. Phys. Chem. A 2016, 120, 4683−4692

(53) (a) Pacifici, L.; Pastore, M.; Garcia, E.; Laganà, A.; Rampino, S. A dynamics investigation of the C + $CH^+ \rightarrow C_2^+$ + H reaction on an ab initio bond-order like potential. *J. Phys. Chem. A* **2016**, DOI: 10.1021/acs.jpca.6b00564. (b) Rampino, S.; Pastore, M.; Garcia, E.; Pacifici, L.; Laganà, A. On the temperature dependence of the rate coefficient of formation of C_2^+ from C + CH^+. *Mon. Not. R. Astron. Soc.* **2016**, DOI: 10.1093/mnras/stw1116.
(54) Pauling, L. Atomic Radii and Interatomic Distances in Metals. *J. Am. Chem. Soc.* **1947**, *69*, 542−553.
(55) Laganà, A. A rotating bond order formulation of the atom diatom potential energy surface. *J. Chem. Phys.* **1991**, *95*, 2216−2217.
(56) Garcia, E.; Laganà, A. Diatomic potential functions for triatomic scattering. *Mol. Phys.* **1985**, *56*, 621−627.
(57) Garcia, E.; Laganà, A. A new bond-order functional form for triatomic molecules. *Mol. Phys.* **1985**, *56*, 629−639.
(58) Laganà, A.; Ochoa de Aspuru, G.; Garcia, E. The largest angle generalization of the rotating bond order potential: Three different atom reactions. *J. Chem. Phys.* **1998**, *108*, 3886−3896.
(59) Laganà, A.; Crocchianti, S.; Faginas Lago, N.; Pacifici, L.; Ferraro, G. A Nonorthogonal Coordinate Approach to Atom-Diatom Parallel Reactive Scattering Calculations. *Collect. Czech. Chem. Commun.* **2003**, *68*, 307−330.
(60) Rampino, S.; Laganà, A. Bond order uniform grids for quantum reactive scattering. *Int. J. Quantum Chem.* **2012**, *112*, 1818−1828.
(61) It is worth noting here that SRBO variables including the whole accessible physical space may be defined by taking $r_{max} = \infty$ ($n_{min} = 0$) and $r_{min} = 0$ ($n_{max} = e^{\beta r_e}$).
(62) Morse, P. M. Diatomic Molecules According to the Wave Mechanics. II.Vibrational Levels. *Phys. Rev.* **1929**, *34*, 57−64.
(63) Collins, M. A.; Zhang, D. H. Application of interpolated potential energy surfaces to quantum reactive scattering. *J. Chem. Phys.* **1999**, *111*, 9924−9931.
(64) Collins, M. A. Molecular potential-energy surfaces for chemical reaction dynamics. *Theor. Chem. Acc.* **2002**, *108*, 313−324.
(65) Frankcombe, T. J.; Collins, M. A.; Worth, G. A. Converged quantum dynamics with modified Shepard interpolation and Gaussian wave packets. *Chem. Phys. Lett.* **2010**, *489*, 242−247.
(66) Ishida, T.; Schatz, G. C. A local interpolation scheme using no derivatives in quantum-chemical calculations. *Chem. Phys. Lett.* **1999**, *314*, 369−375.
(67) Maisuradze, G. G.; Thompson, D. L.; Wagner, A. F.; Minkoff, M. Interpolating moving least-squares methods for fitting potential energy surfaces: Detailed analysis of one-dimensional applications. *J. Chem. Phys.* **2003**, *119*, 10002−10014.
(68) Aguado, A.; Suárez, C.; Paniagua, M. Accurate global fit of the H_4 potential energy surface. *J. Chem. Phys.* **1994**, *101*, 4004−4010.
(69) Tablero, C.; Aguado, A.; Paniagua, M. Global fit of ab initio potential energy surfaces: II.2. Tetratomic systems A_2B_2 and ABC_2. *Comput. Phys. Commun.* **2001**, *140*, 412−417.
(70) Aguado, A.; Tablero, C.; Paniagua, M. Global fit of ab initio potential energy surfaces: II.1. Tetraatomic systems ABCD. *Comput. Phys. Commun.* **2001**, *134*, 97−109.
(71) Sorbie, K. S.; Murrell, J. N. Analytical potentials for triatomic molecules from spectroscopic data. *Mol. Phys.* **1975**, *29*, 1387−1407.
(72) Werner, H.-J.; Knowles, P. J.; Knizia, G.; Manby, F. R.; Schütz, M.; Celani, P.; Korona, T.; Lindh, R.; Mitrushenkov, A.; Rauhut, G. et al. MOLPRO, version 2010.1, a package of ab initio programs. 2010; see http://www.molpro.net, Accessed October 9, 2015.
(73) Dunning, T. H. Gaussian basis sets for use in correlated molecular calculations. I. The atoms boron through neon and hydrogen. *J. Chem. Phys.* **1989**, *90*, 1007−1023.
(74) Skouteris, D.; Castillo, J. F.; Manolopoulos, D. E. ABC: a quantum reactive scattering program. *Comput. Phys. Commun.* **2000**, *133*, 128−135.
(75) A Fortran computer program for constructing SRBO grids is available at http://www.srampino.com/code.html#Pestk or upon request to info@srampino.com.
(76) Liu, B. Ab initio potential energy surface for linear H_3. *J. Chem. Phys.* **1973**, *58*, 1925−1937.
(77) Siegbahn, P.; Liu, B. An accurate three-dimensional potential energy surface for H_3. *J. Chem. Phys.* **1978**, *68*, 2457−2465.
(78) Truhlar, D. G.; Horowitz, C. J. Functional representation of Liu and Siegbahn's accurate ab initio potential energy calculations for H + H_2. *J. Chem. Phys.* **1978**, *68*, 2466−2476.
(79) Truhlar, D. G.; Horowitz, C. J. Erratum: Functional representation of Liu and Siegbahn's accurate abinitio potential energy calculations for H + H_2. *J. Chem. Phys.* **1979**, *71*, 1514−1514.
(80) Varandas, A. J. C.; Brown, F. B.; Mead, C. A.; Truhlar, D. G.; Blais, N. C. A double many-body expansion of the two lowest-energy potential surfaces and nonadiabatic coupling for H_3. *J. Chem. Phys.* **1987**, *86*, 6258−6269.
(81) Boothroyd, A. I.; Keogh, W. J.; Martin, P. G.; Peterson, M. R. An improved H3 potential energy surface. *J. Chem. Phys.* **1991**, *95*, 4343−4359.
(82) Boothroyd, A. I.; Keogh, W. J.; Martin, P. G.; Peterson, M. R. A refined H_3 potential energy surface. *J. Chem. Phys.* **1996**, *104*, 7139−7152.
(83) Mark Wu, Y.-S.; Kuppermann, A.; Anderson, J. B. A very high accuracy potential energy surface for H_3. *Phys. Chem. Chem. Phys.* **1999**, *1*, 929−937.
(84) Peterson, K. A.; Woon, D. E.; Dunning, T. H. Benchmark calculations with correlated molecular wave functions. IV. The classical barrier height of the H + $H_2 \rightarrow H_2$ + H reaction. *J. Chem. Phys.* **1994**, *100*, 7410−7415.
(85) Xie, Z.; Bowman, J. M. Permutationally Invariant Polynomial Basis for Molecular Energy Surface Fitting via Monomial Symmetrization. *J. Chem. Theory Comput.* **2010**, *6*, 26−34.
(86) Zhu, X.; Yarkony, D. R. Fitting coupled potential energy surfaces for large systems: Method and construction of a 3-state representation for phenol photodissociation in the full 33 internal degrees of freedom using multireference configuration interaction determined data. *J. Chem. Phys.* **2014**, *140*, 024112.
(87) Garcia, E.; Martínez, T.; Laganà, A. Quasi-resonant vibrational energy transfer in N_2 + N_2 collisions: Effect of the long-range interaction. *Chem. Phys. Lett.* **2015**, *620*, 103−108.
(88) Garcia, E.; Sánchez, C.; Rodríguez, A.; Laganà, A. MEP-MPE potential energy surface for the Cl + $CH_4 \rightarrow$ HCl + CH_3 reaction. *Int. J. Quantum Chem.* **2006**, *106*, 623−630.

NOTE ADDED AFTER ASAP PUBLICATION

This article was published ASAP on December 29, 2015, with an incomplete version of ref 53. The corrected version was published ASAP on May 23, 2016.

DOI: 10.1021/acs.jpca.5b10018
J. Phys. Chem. A 2016, 120, 4683−4692